Research Article

Carlo E.D. Riboldi*, Lorenzo Trainelli, Luca Mariani, Alberto Rolando, and Francesco Salucci

Predicting the effect of electric and hybrid-electric aviation on acoustic pollution

https://doi.org/10.1515/noise-2020-0004
Received Dec 19, 2019; accepted Feb 20, 2020

Abstract: In the quest for the reduction of noise pollution, novel hybrid-electric or fully-electric power-trains promise to provide a substantial contribution. Especially closer to airfields, where acceptability issues tend to limit air operations with conventional fuel-burning engines, such novel power-trains allow to fly terminal maneuvers with a dramatically reduced impact on pollution. Considering the General Aviation (GA) field, where such new types of propulsion are more likely to gain a significant market share thanks to their favorable characteristics for this weight category, the reduction of the noise impact on ground may increase the infrastructural value of smaller airfields, often located in densely populated areas. This in turn would help in making novel power-train technologies economically advantageous at a system level. Despite these evident advantages, a methodology to quantify noise emissions of a novel type of power-train has not been identified yet – a fundamental step towards the assessment of the potential contribution of hybrid-electric or fully-electric aircraft to the global scenario of future aviation. This work introduces and discusses a possible procedure to provide such estimation. While mainly focused on the field of propeller-driven GA aircraft, the procedure presented herein can be easily scaled to cope with the specific features of heavier categories.

Keywords: hybrid-electric aircraft, noise prediction, noise sources, source-blending method

***Corresponding Author: Carlo E.D. Riboldi:** Department of Aerospace Science and Technology, Politecnico di Milano, Italy; Email: carlo.riboldi@polimi.it
Lorenzo Trainelli, Luca Mariani, Alberto Rolando, Francesco Salucci: Department of Aerospace Science and Technology, Politecnico di Milano, Italy

1 Introduction

The reduction of noise pollution in areas close to airfields is among the most significant improvements promised by a transition to fully-electric or hybrid-electric propulsion in aviation. The ability of electric or hybrid-electric aircraft to operate without the support of a hydro-carbon fuel-burning engine in terminal maneuvers, *i.e.* during take-off/climb-out or approach/landing, allows to reduce noise emission in proximity to the ground, where these may turn more annoying and harmful.

For conventionally propelled aircraft, methods for predicting the aircraft-borne noise perceived on ground are many, and well documented in the literature as well as in regulation and best-practice manuals. They will be quickly revised in the next paragraph 1.1.

1.1 State of the art

The intensity and contours of the noise footprint on ground can be computed together by applying dedicated comprehensive models, considering the aircraft as a single point emitter. The map of noise emissions can be assessed for comparisons and regulation compliance purposes in test conditions suggested through best-practices.

Two classes of such comprehensive models exist, based on either a semi-empirical or theoretical approach. Concerning semi-empirical, best-practice models, for many existing aircraft, the ANP database [1] produced by EUROCONTROL offers self-contained methods for designing a test terminal trajectory and predict the corresponding noise emissions. That estimation methodology complies with the guidelines for airport noise assessment approved by ECAC [2], which in turn are derived from ICAO regulations [3]. Similar methods have been developed in several European Countries (implemented in suites like ANCON [4], FLULA [5], SIMUL [6] or AzB [7]), where they are currently used for regulation compliance assessment. Further noise prediction methods are part of suites capable of predicting also chemical pollution (IESTA [8], IMPACT [9] and AEDT [10]).

Due to the complexity and computational effort associated to sound propagation phenomena, some models based on a theoretical approach do make use of empirical methods for internal sub-tasks, for the computation of the noise footprint over a larger area. Among the most complete suites of methods worth citing are ANOPP2 [11] developed by NASA, and PANAM [12] of the DLR.

Theoretical methods usually consider separate sources of noise, which are studied one by one and combined *a posteriori*, to bear a prediction corresponding to the whole aircraft. To this end, models for each major source of noise on-board the aircraft are needed. The abundant available research works in this area can be categorized based on the sources they analyze.

Propeller noise has been studied since many decades, and models unanimously split this effect into a prevailing tonal component [13] and a background broad-spectrum noise [14, 15]. The interference of propeller and airframe has also been analyzed, concerning its tonal contribution [16, 17]. Best-practice methods as usual require a lower computational effort and allow for an easier implementation [18–20].

Comparatively fewer models exist for noise bound to airframe and landing systems, *i.e.* landing gear and high-lift devices. A few semi-empirical models for the airframe and the fixed part of the wing are rather widespread, some with a good level of applicability which allows an easier application to diverse sub-sources of noise [21], whereas others feature a more limited theoretical generality [22]. Wing noise, mostly bound to turbulent kinetic energy scattering at the trailing edge of the wing, has been studied more in depth [23, 24], similarly to flap- [25, 26] and slat-related noise [27, 28]. Only empirical models exist for landing gear noise [29].

Considering engine noise, the most recent works deal with jet applications, whereas piston engines have received little attention - despite being of much greater relevance for the application of novel propulsive technologies in aviation, more likely to appear in the lower aircraft weight category in substitution of piston engines. Nonetheless, analyses carried out in the automotive field have shown that the most relevant engine-related noise component is due to aerodynamics, and connected with intake and exhaust flows. Very accurate models in this field [30–33] are possibly less suitable than easier, semi-empirical models [34–37] at least in the initial phases of aircraft design, due to the uncertainty on input values typical to this stage.

While not so intense as the sources of noise cited above, also the contributions of electric motors and gearboxes have been studied. For the former, besides detailed models based on FEM/BEM analyses, more compact and usable models are based on a statistical approach. For gearboxes, the main emission modes of whine and rattle can be modeled by means of statistical energy methods [38, 39]. The complexity of the vibration and propagation phenomena often requires simplifications to increase generality and usability, at the price of accuracy. Models based on such simplifications are conveyed in more widespread empirical formulations [40–42], sometimes presented in an integrated fashion for more sources [43].

1.2 Issues and proposed methodology

The cited references provide comprehensive procedures for noise prediction especially useful in close proximity to airports, as long as fuel-burning aircraft are considered, whereas documented source-related models deal with the prediction of noise emitted by components of an aircraft (*e.g.* airframe, wing, landing gear) or a power-train, never considering the aircraft as a whole.

Notwithstanding the available knowledge-base, due to the relative immaturity of electric and hybrid-electric aviation for which scant data is available, no best-practices or consolidated procedures exist dealing with the prediction of noise emission of an electric or hybrid-electric aircraft. This hampers a straightforward and accurate quantification of the noise foot-print on ground for these novel types of aircraft. A similar tool would be extremely valuable, to better assess the potential contribution of new propulsion systems in terms of environmental impact and public acceptability, already at a design level working in a virtual environment.

The research presented herein tries to fill this gap, describing a prediction methodology for noise emissions for aircraft, applicable not only to more usual fuel-burning models, but also to innovative fully-electric or hybrid-electric aircraft.

The methodology starts from the selection and refinement of existing models predicting the noise emissions from some of the most relevant sources in a typical aircraft design.

Considering in a preparatory phase fuel-burning aircraft, for which data and procedures for estimating the overall noise footprint indeed exist, the noise produced by each source in a simulated validation scenario is combined at first in a brute force fashion, showing how this approach does not bear accurate results when compared to the reference. Secondarily, the sources are combined based on an optimal approach, so as to obtain a total figure which fits in the best possible way the prediction of a con-

solidated, comprehensive model. It will be shown how this model-fitting procedure will produce an estimation model blending the output of the different sources, directly applicable to a broad set of existing aircraft yielding accurate predictions.

In view of the state-of-the-art of innovative propulsion, new electric or hybrid-electric aircraft are more likely to appear in the General Aviation category, which has been considered for validating and further testing the novel source-blending procedure, without loss of generality from a methodological standpoint.

Once the relative weight of each source has been defined to bear a statistically accurate prediction of the total noise produced by a standard aircraft, an application to the case of the Pipistrel Panthera is presented. This aircraft is already in production in a usual fuel-burning version, while a hybrid-electric variant is currently in the design phase, among the first such aircraft likely to enter production soon. The sources of noise differ between the two variants, which nonetheless share most macroscopic features in their configuration.

The results of a comparison of noise emissions, carried out simulating the real case of terminal maneuvers around Milan-Bresso Airport (ICAO: LIMB, located north of downtown Milan), based on realistic trajectory data and using the presented novel prediction procedures, will be considered to put forward some speculations about the effectiveness of hybrid-electric propulsion in reducing noise emissions.

1.3 Structure of this paper

The paper is organized as follows. The models considered for the source-blending method are presented component by component, as well as a comprehensive model needed for the validation of the method. The novel source-blending method is thoroughly validated, and its accuracy assessed, with respect to the comprehensive approach, showing its ability to correctly predict the noise of fuel-burning aircraft. Finally, the potential of the source-blending method is shown through some specific comparative analyses on hybrid-electric aircraft in the realistic case of circuit-flying over an existing General Aviation airport.

2 Modeling noise emissions

2.1 Baseline comprehensive prediction method

A reliable baseline and term of comparison for setting up and validating a novel noise prediction procedure is the monolithic procedure proposed by ECAC Report Doc. 29 [2]. This is currently being adopted by many national aviation regulation agencies for assessing the noise emissions in the vicinity of aerodromes, as per the European Regulation No. 598/2014 [44], explicitly citing it as a procedure for monitoring compliance on existing airports.

2.1.1 Trajectory definition

The basic concept behind the modeling proposed as a best-practice in prediction procedures by ECAC is that of considering separately departure and arrival phases, and of providing for each of them a suitable segmentation of the maneuver. Segmentation refers primarily to a non-uniform discretization of the geometrical trajectory in straight segments, but also to the definition of nodal values of flight mechanics parameters, namely available power, true airspeed and bank angle. Specified for the boundary nodes of each segment of the trajectory, these reference values are employed to compute a reference for the whole corresponding segment. For many existing aircraft, the Aircraft, Noise and Performance (ANP) database [1] allows to obtain by means of look-up tables noise-power-distance (NPD) data. These include maximum A-weighted sound pressure levels (SPL) and sound exposure levels (SEL), provided for each specific aircraft model as functions of an assigned set of output power and emitter-receiver slant distance values. Once the trajectory is assigned, for a receiver in a fixed position on ground it is possible to measure the contribution of each segment of a trajectory in terms of maximum SPL and SEL, by properly navigating the ANP database, interpolating where necessary. Furthermore, by suitably mixing the contributions of each segment in a terminal maneuver, it is possible to assess its associated overall maximum SPL and SEL for an assigned sensor.

In order to better explain the construction and features of the baseline ECAC model, we introduce the example of the Milan-Bresso Airport, a General Aviation airport located north of Milan, Italy, and already considered for other related projects concerned with transition to novel aircraft propulsion technologies [45]. Considering the ground track, *i.e.* the projection of the terminal trajec-

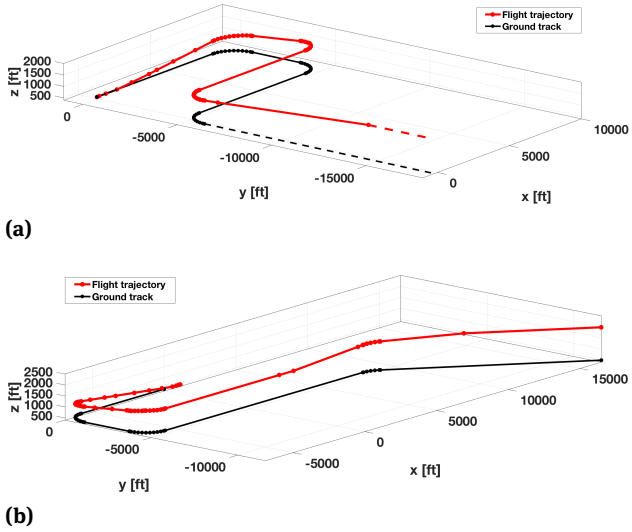

Figure 1: Three-dimensional trajectories for (a) departure and (b) arrival. Milan-Bresso RWY18 right-hand standard circuit. Discretization based on ECAC prescription for noise emission analysis, considering flight performance of a Cessna C172R Skyhawk.

tories on ground, represented by the (x,y) plane, according to ECAC guidelines, segments corresponding to curved trajectories have been modeled considering a maximum corresponding turn angle of 10 deg. Concerning the vertical dimension (z), the flight profile is described by means of a geometrical trajectory, as well as speed and thrust (which implicitly provide power) associated to each segment node. A trajectory for a specific aircraft model can be assembled based on corresponding average flight mechanics data. Discretization following the guidelines of ECAC imposes the addition of nodal points corresponding to every change in power setting, as well as for changes of speed reaching up to 10 m/s. As a result, nodes are not matching *a priori* for the ground track and vertical profile. All nodes from both discretizations are considered in the final three-dimensional discretization.

Considering the case of a Cessna C172R Skyhawk [46], a model usually operating from Milan-Bresso airfield, Figure 1 shows the result for standard RWY18 right-hand circuit departure and arrival procedures.

2.1.2 Computation of noise emission via baseline method

As recalled, a comprehensive measure of noise emission associated to a terminal maneuver can be computed by means of two indicators, namely maximum SPL (symbol L_m in equations) and SEL (symbol L_E in equations), captured by a noise sensor located in an arbitrary position on the (x,y) plane. Based on ECAC best-practices, from the nodal values around each segment along the trajectory, it is possible to select a single set of power, speed, and bank angle values, representative of the motion of the aircraft along that segment. Adding to the set a reference measure of slant distance between the segment and sensor on ground, the contribution of each j-th segment to the overall noise perceived by the sensor can be computed in terms of $L_{m,j}$ and $L_{E,j}$ as follows [2]

$$L_{m,j} = L_m(P, d) + \Delta_I - \Lambda(\beta, l) + \Delta_S \qquad (1)$$
$$L_{E,j} = L_E(P, d) + \Delta_V + \Delta_I - \Lambda(\beta, l) + \Delta_F + \Delta_S.$$

In Eq. 1, quantities $L_m(P, d)$ and $L_E(P, d)$ can be obtained from the ANP database, as functions of the power available P and slant distance between the segment and the sensor d. Both measures in Eq. 1 are corrected by several effects, accounted for by the other components appearing in the corresponding expressions. The term Δ_I accounts for the effect of engine position in the aircraft configuration. However, as per ECAC prescription, this should be accounted for only in jet-propelled aircraft. As stated in the introduction, such propulsion type is not treated in this research, hence $\Delta_I = 0$ except for the validation of the implementation shown in section 2.1.3. The term $\Lambda(\beta, l)$ represents lateral attenuation, and is a function of the elevation angle β between the direct sound propagation path and the ground, and of the lateral displacement of the observer from the ground track l. The Δ_S term accounts for the strong directionality of exhaust plumes of jet engines at high thrust settings, but it is null for propeller-driven aircraft ($\Delta_S = 0$). Again, it will be considered only for validation (section 2.1.3).

Terms which impact only on the SEL are firstly Δ_V, a speed correction factor accounting for the ratio between the actual airspeed in the nodal points along the trajectory and the reference airspeed $V = 160$ kn adopted in the ANP database. Similarly, Δ_F accounts for the limited length of each segment in the trajectory, in view of the ideal infinite-length trajectories considered for the setup of the ANP database. This term yields a decrease in SEL, on account of the limited actual time needed to fly each segment.

2.1.3 Validation of the baseline method

A tool for validating a novel implementation of the ECAC method is provided by the Volume 3 of ECAC Doc. 29 [47]. The document defines a series of test cases. Three aircraft with assigned data are considered, a jet-powered aircraft with underwing engines (JETW), one with tail engines

Table 1: Results of the validation of a novel implementation for a baseline estimation method wrt. ECAC reference. Values in dB. All values are below 0.01 dB accuracy tolerance.

	Departure (straight)	Departure (with turn)	Approach (straight)	Approach (with turn)
JETF	$2.99e^{-3}$	$3.11e^{-3}$	$2.84e^{-3}$	$2.89e^{-3}$
JETW	$2.99e^{-3}$	$3.04e^{-3}$	$2.98e^{-3}$	$2.97e^{-3}$
PROP	$3.00e^{-3}$	$3.19e^{-3}$	$2.83e^{-3}$	$2.85e^{-3}$

(JETF), and a propeller-driven aircraft (PROP). All three are checked over four assigned trajectories, two departures and two approaches, either straight or involving a turn.

In a first stage, noise sensors are positioned in 18 predetermined locations, and SEL measured and compared to provided reference values for each of them. The contribution to SEL, in particular the various corrective components shown in Section 2.1.2, are checked separately, and considering the trajectory segments one by one (see 2.1.1). In the final stage of the validation, the measurements are carried out on a more refined grid, covering a broader geometric extension. The adopted validation metric is related to the difference between the measured SEL $L_{E,k}$ and the reference $\overline{L_{E,k}}$, as per the following definition

$$\delta = \sqrt{\frac{\sum_{k=1}^{N_S}(L_{E,k} - \overline{L_{E,k}})^2}{N_S}}, \tag{2}$$

where N_S is the number of sensors in the grid. Table 1 shows the deviation between the ECAC reference and our implementation, needed for the development of original models later presented in this work.

It can be noticed that the results are all largely lower than 0.01 dB required for model compliance. It is henceforth assumed that the baseline ECAC method in our implementation can be considered ground-truth for the next steps.

2.2 Source-bundling prediction method

As explained in the introduction (see 1.2), the baseline method just discussed makes use of pre-computed noise emission data provided in the ANP database. An issue arises when novel aircraft are considered that are not included in the database. Especially for electric or hybrid-electric aircraft of interest here, due to the scant number of well-developed designs and exemplars flying today, such data is not available. An alternative way to estimate the overall noise emitted by an aircraft, and the corresponding SPL and SEL on ground, is that of bundling together the contributions of the noise sources on board.

As observed in the overview on the state of the art (see 1.1), there are usually more models available for the prediction of noise emissions from each considered source. These can be roughly divided into theoretical models, based on an analytic approach starting from balance principles applied to fluid dynamics, and semi-empirical models, based on a less accurate analytic description of the emission and propagation phenomena, but supported by substantial corrections based on experimental data. The latter type has been deemed generally more suitable to the problem under analysis. This is due to at least two reasons. Firstly, models starting from a theoretical approach are invariably dependent on a significant number of parameters, which are not often available at a design level, or affected by significant uncertainty. Secondarily, the computational cost of theoretical methods makes them further unsuitable for a preliminary design analysis, where the chance to quickly predict performance changes with respect to a baseline, by means of extensive parameterized analyses, is more relevant than a very high accuracy.

The models selected for an estimation of the overall emission following the source-bundling approach are listed below.

2.2.1 Selection of prediction models for different sources

As for the propeller, suitable available models have been proposed by Smith [48], by Rathgeber [19] and in the SAE AIR1407 [18]. Smith's model and SAE AIR1407 provide results more similar to one another also in terms of accuracy, whereas the likelihood of the output of Rathgeber's equation is generally lower. However, Smith's model requires propeller data (thickness-to-chord ratio and twist at some specific radii from the propeller hub) which are not commonly available at the preliminary design stage. Therefore, SAE AIR1407 has been selected for this work.

Based on the adopted formulation, far-field propeller noise is computed on the basis of a set of partial levels and correction factors, estimated from the basic configuration and operating parameters of the propeller. In particu-

lar, the inputs are represented by some geometrical parameters (propeller diameter, number of blades and number of propellers), quantities describing the equilibrium condition (propeller rotational speed, power input and flight speed) and the environmental condition (ambient temperature). The final input is of course given by the slant distance between the aircraft and sensor, and the elevation angle between the ground and the aircraft-sensor line of propagation. Once singularly determined, a number of partial noise terms and corrections are combined arithmetically to obtain the A-weighted SPL pertaining to a specific aircraft position.

The choice of a prediction model for airframe noise is more limited, especially for propeller-driven aircraft of interest in this work. The model presented by Fink [21] is nonetheless of general applicability, and particularly useful especially for it provides simple, separate models for the wings, flaps, slats and landing gear. Similarly ready-to-use methods are presented in ESDU 90023 [49], which is nonetheless not applicable to propeller-driven aircraft.

Focusing on Fink's model, the A-weighted SPL values due to the wing, horizontal and vertical empennages are estimated from their respective surface and span. The same holds for deployed slats, whereas trailing edge flap noise requires the flap deflection angle too as an input. As for landing gear instead, the number of wheels per gear assembly, as well as the diameter of the tyre, is considered for noise computation. Clearly, the noise of all sources in Fink's model is also a function of the relative position between the aircraft and the ground sensor. The contribution of the different sources is then summed on an energetic basis to obtain the A-weighted SPL bound to the airframe noise.

Considering engine noise, for piston engines in the aeronautical field the formulation proposed by Dobrzynski and reported by Tada [36], is more general than Moshkov's model [37], which is applicable only to a set of specific engines.

According to Dobrzynski's formulation, engine noise in terms of A-weighted SPL is computed from the actual and maximum rotational speed of the engine, from the maximum engine power, and clearly from the slant distance between the aircraft and the sensor on ground.

Concerning the electric motor and gearbox, readily applicable models compatible with the current aeronautical application - *i.e.* power levels and power-to-weight ratios in the same range of existing electric or hybrid-electric designs - are reported in the work by Bruce [43].

For electric motors, the prediction is provided in terms of sound power level L_w starting from the motor size, rotational speed and power output. Considering the relationship between acoustic power and pressure, this estimation can be translated into an instantaneous value L_p of the distance-dependent SPL by assuming a point-source model for the motor, by means of the transformation

$$L_p = L_w + 10 \log_{10} \left(\frac{Q}{4\pi r^2} \right), \tag{3}$$

where Q is a shape parameter defined as the ratio between a spherical area of radius r and the actual area over which spreading is taking place instant by instant - so that if the measurement area is spherical, $Q = 1$.

As for the gearbox, the sound power level can be computed based on the semi-empirical model expressed as

$$L_w = 86 + 3 \log_{10} N + 4 \log_{10} P_w + 10 \log_{10} S, \tag{4}$$

where N is the rotational speed of the shaft, P_w is power transferred by the gearbox, and S a conformal surface measured at one meter from the gearbox, computed from basic geometrical data of the gearbox assembly [43]. The same Eq. 3 can be used for spatial propagation.

2.2.2 Bundling sources: methodological issues

The source-bundling method is centered on the concept that the total noise emission of the aircraft, measured in energy terms through the SPL L_p^{AC}, where superscript AC stands for "aircraft", should be obtained by simply summing the noise emitted from all sources on board the aircraft. For a conventionally propelled aircraft, these are namely the airframe, which includes the wing/tail assemblies, deployable surfaces and landing gear, the propeller and the engine. When novel propulsion systems are considered, the electric motor and gearbox are further sources to be considered.

However, the models selected for each noise source are not fully compatible in terms of output.

In particular, the model for airframe noise produces spectral values of the SPL $L_{p,n}$, *i.e.* spectra of sound pressure levels evaluated at each one-third of octave band. The effect of spacial attenuation, *i.e.* decrease in noise power density as the distance from the source increases, is correctly accounted for by the model (see Eq. 3). Instead, the effect of atmospheric absorption, which translates into a pure energy loss, is not accounted for. This is true except for the wing sub-part, where also atmospheric absorption is accounted for in the model.

In order to correct the output of the airframe model accounting for atmospheric absorption, SAE AIR1845 [50] defines the following model

$$L_{p,n_\alpha} = L_{p,n} - \alpha_n d, \tag{5}$$

where the absorption-attenuated, frequency-dependent value of the SPL spectrum L_{p,n_α} is obtained from the unattenuated $L_{p,n}$ value, through a correction accounting for the distance between the source and measurement point d and an atmospheric absorption coefficient α_n.

Differently from the airframe case, the adopted model for propeller noise produces SPL values which correctly account also for atmospheric attenuation [18].

The models for the engine, electric motor and gearbox all produce an overall SPL, *i.e.* a quantity not depending on frequency, and unattenuated with respect to atmospheric absorption. This hampers the direct use of Eq. 5. However, ECAC Doc. 29 provides the means to account for atmospheric absorption [2]. Among the data provided in the ANP database, spectral values of SPL $L_{p,n_\alpha}(\bar{d})$ are reported for a slant distance of $\bar{d}$ = 1 000 ft, and already corrected recurring to SAE AIR1845 method. Values are listed depending only on aircraft size, and can therefore be adopted without precisely accounting for the power-plant. By inverting Eq. 5, it is possible to obtain first the unattenuated value $L_{p,n}(\bar{d})$. Secondarily, the following equation can be adopted to obtain the spectral SPL information as a function of a generic slant distance d

$$L_{p,n}(d) = L_{p,n}(\bar{d}) - 20\log_{10}\left(\frac{d}{\bar{d}}\right). \tag{6}$$

Finally, the SPL accounting for atmospheric absorption $L_{p,n_\alpha}(d)$ can be computed according to Eq. 5.

Given the values of $L_{p,n_\alpha}(d)$ and $L_{p,n}(d)$, the effect of noise absorption on the overall SPL can be estimated from the following expression

$$\begin{aligned}\Delta L_p(d) =& 10\log_{10}\left(\sum_n 10^{\frac{L_{p,n_\alpha}(d)+A_n}{10}}\right) \\ &- 10\log_{10}\left(\sum_n 10^{\frac{L_{p,n}(d)+A_n}{10}}\right),\end{aligned} \tag{7}$$

where the spectral values of the SPL $L_{p,n_\alpha}(d)$ and $L_{p,n}(d)$ are A-weighted, energetically summed over frequency, and the results subtracted to one another.

The so-obtained value provides an estimation of the absorption term on the global SPL, not depending on frequency, which is applied to the noise contributions of the engine, electric motor and gearbox, making the output of the respective models compatible with that of propeller and airframe sources (the latter suitably treated as described above).

Now the global SPL from all sources $L^{AC}_{p,A}(d)$ can be obtained through an energetic sum of the A-weighted SPL values pertaining to each source, as

$$\begin{aligned}L^{AC}_{p,A}(d) = 10\log_{10}\Bigg(&\sum_n 10^{\frac{L^a_{p,n_\alpha,A}(d)}{10}} + 10^{\frac{L^p_{p_\alpha,A}(d)}{10}} + \\ &10^{\frac{L^e_{p_\alpha,A}(d)}{10}} + 10^{\frac{L^m_{p_\alpha,A}(d)}{10}} + 10^{\frac{L^g_{p_\alpha,A}(d)}{10}}\Bigg),\end{aligned} \tag{8}$$

where $L^a_{p,n_\alpha,A}(d)$ represents the spectral information of the SPL pertaining to the n-th frequency considered, accounting for atmospheric absorption (subscript α), A-weighted (subscript A) and due to the airframe (superscript a). Due to the differences in the output between the airframe model - which produces a frequency distribution - and those for the propeller, engine, electric motor and gearbox, the respective $L^p_{p_\alpha,A}(d)$, $L^e_{p_\alpha,A}(d)$, $L^m_{p_\alpha,A}(d)$, $L^g_{p_\alpha,A}(d)$ terms, representing overall SPL values, are included in Eq. 8 instead of frequency-dependent quantities.

2.2.3 Validation of source-bundling prediction method

In order to assess the accuracy of the source-bundling method, a procedure has been devised where the NPD data contained in the ANP database provided by ECAC [47] are used as a reference. These data refer to noise levels registered on ground during flyover tests at ten reference slant distances between 200 ft and 25 000 ft. Flyover tests have been performed at an airspeed of 160 kn, and for at least four different power settings, of which two corresponding to approach procedures, two to departure procedures. In the intention of the designers of the database, these test conditions should provide results representative of terminal maneuvers in different aircraft configurations (*i.e.* different power settings, landing gear extension, flap deployment). The measured quantity is the SEL of the whole aircraft, $L_{E,A}$, defined as

$$L_{E,A}(d) = 10\log_{10}\left(\int_{t_1}^{t_2} 10^{\frac{L^{AC}_{p,A}(d,t)}{10}}\,\mathrm{d}t\right). \tag{9}$$

Clearly, the actual value of $L_{E,A}(d)$ for an assigned slant distance d depends on the considered values of t_1 and t_2. The SEL values reported in the ANP database refer to the time instants when the A-weighted SPL of the aircraft $L^{AC}_{p,A}(d, t)$ during a test overflight is above 10 dB from the maximum recorded during the flyover.

The validation of the source-bundling method was carried out on several aircraft models, including single and multiple-engine, available in the database. As an example, the values of $L_{E,A}$ obtained for a Cessna C172R [46] are presented in Figure 2. This aircraft is of special relevance

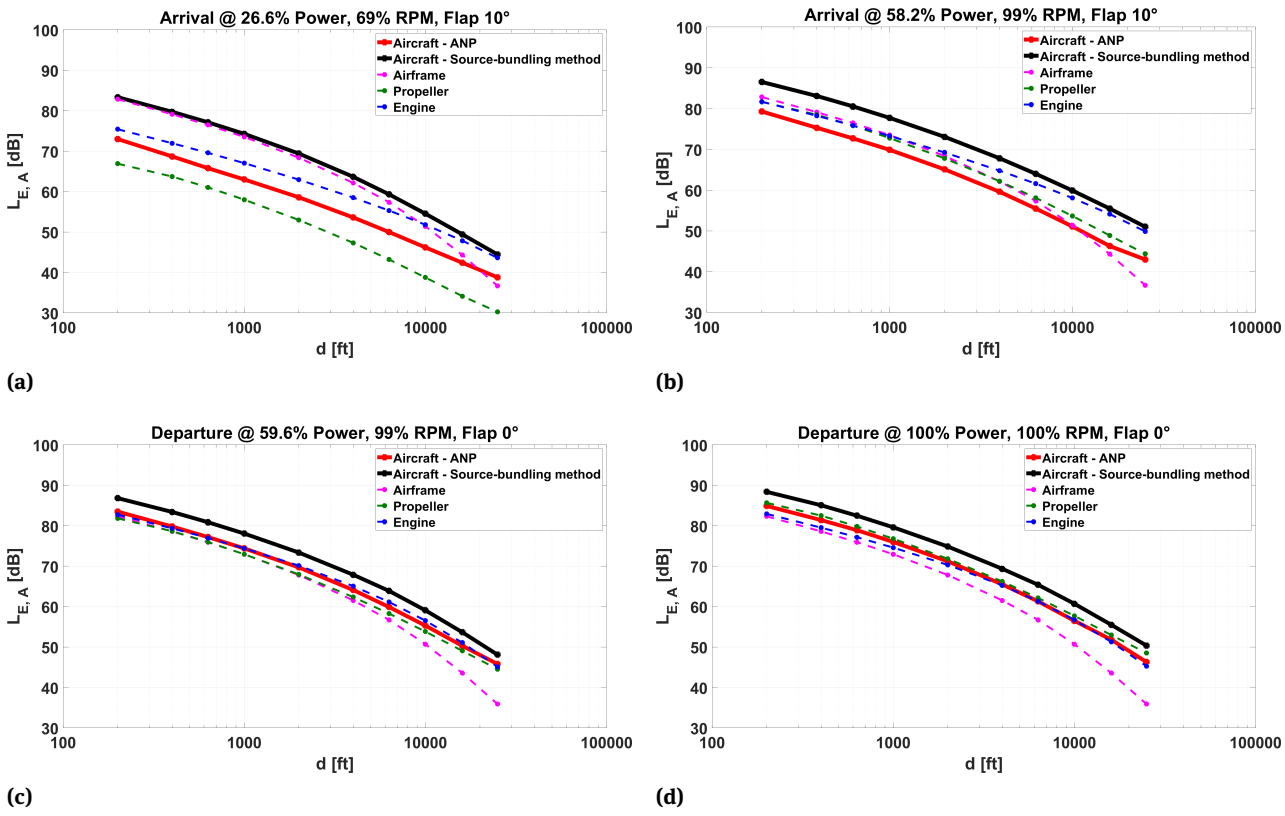

Figure 2: Comparison of SEL data from ANP database and predictions obtained from the source-bundling method for a Cessna C172R during overflight missions, for method validation. (a,b) arrival procedures. (c,d) departure procedures.

in the present study, for this is the model in the database more often operating from Milan-Bresso. The SEL values pertaining to a set of slant distances during the overflight are displayed. On the top row of Figure 2 are presented results for arrival procedures, whereas results for departure are shown on the bottom row. The red line in these plots refers to database SEL data.

An issue related to the validation procedure is the lack of information in the description of the ANP database concerning aircraft configuration and engine settings adopted for flyover tests. Reasonable configuration settings have been retrieved from flight manuals. In particular, take-off and landing flap settings have been adopted for the database entries corresponding to departure at maximum power (a typical short-distance take-off configuration) and landing at minimum power respectively. Climb-out and approach flap settings have been considered for lower power take-off and high-power landing entries respectively. For the case of the Cessna C172R in Figure 2, the contribution of the landing gear is always present, due to the fixed undercarriage configuration of the aircraft. In other validation cases with retractable gear (not presented), the noise contribution of the landing gear has been accounted for only in the entries corresponding to take-off at high-power and landing at low-power.

Concerning the propeller and engine, the ANP database provides either the rotational speed or the net thrust for each flyover, depending on the selected aircraft. The model for noise emission of the propeller is fed by input power and rotational speed, whereas for the engine the model needs as inputs maximum power, current and maximum rotational speed. Assuming a constant airspeed of 160 kn and a constant propeller efficiency, it is possible to compute matching values of propeller thrust and engine power. Furthermore, the engine database elaborated by Yakovitch [51] allows to extract for several engines matching values of rotational speed and engine power, thus allowing to translate one quantity into the other as required. Such engine operational data are provided for several configurations, namely take-off, climb, cruise, approach and landing. Henceforth, with the addition of sheet data for maximum rotational speed and power for the considered engines, it is possible to translate the data in the ANP database into the required input for the noise emission models of the propeller and engine.

Table 2: Aircraft in the ANP database considered for the design of the blending coefficients in the source-blending method.

Aircraft model	ID	Engines	MTOW [lb]
Piper PA-28-161 Warrior [52]	PA-28	1	2 325
Cessna C172R Skyhawk [46]	C172R	1	2 450
Cessna C182H Skylane [46]	C182H	1	2 800
Cessna C206H Stationair [46]	C206H	1	3 600
Cessna T206H Stationair [46]	T206H	1	3 600
Piper PA-30 Twin Comanche [52]	PA-30	2	3 600
Beechcraft B58P Baron [53]	BB 58	2	6 100
Piper PA-31-350 Navajo Chieftain [52]	PA-31	2	7 000

No electrical motor nor a gearbox are present in the selected validation test-beds, which are based on standard piston engines, hence the corresponding noise sources are not accounted for in this phase.

Recalling Figure 2, the contribution of each component is presented together with the total aircraft emission, resulting from source-bundling (in black on all plots). It can be noticed that the bundling method generally overestimates the ANP value. The error is more marked for arrival procedures, where it is never below 5 dB, and reaches 9.5 dB for the lowest power setting and minimum considered slant distance, where the SEL is most intense. Looking again at arrival procedures, the prediction for some of the sources exceeds the ANP global SEL value.

Considering departures, the picture is only slightly better, with an error between the totals as low as 3 dB, and never exceeding 5 dB. A persistent bias between the two predictions is noticeable for all considered slant distances.

As a remark, it can be observed that no source is constantly prevailing on others, nor are the source predictions providing meaningless or unexpectedly scattered results. This and the (albeit loose) likelihood of the total predicted values for the two methods is in support of a general reliability of the prediction methods adopted for each noise source. Yet the accuracy of the source-bundling method, also due to the basically arbitrary hypotheses needed to obtain values to be fairly compared to the published ANP database, is generally not satisfactory.

2.3 Increasing accuracy: the source-blending method

In order to increase the accuracy of the prediction, a novel method is introduced, where the predictions obtained from the models for each single source are blended together, after modulation through a suitable blending coefficient, yielding the following expression for the SEL

$$L_{E,A}(d) = 10\log_{10}\left(\int_{t_1}^{t_2} 10^{x_1\frac{L^a_{p,A}(d,t)}{10}} + 10^{x_2\frac{L^p_{p,A}(d,t)}{10}} + 10^{x_3\frac{L^e_{p,A}(d,t)}{10}} + 10^{x_4\frac{L^m_{p,A}(d,t)}{10}} + 10^{x_5\frac{L^g_{p,A}(d,t)}{10}}\,\mathrm{d}t\right). \quad (10)$$

The generic blending coefficient x_k, $k = 1, \ldots, 5$, can be interpreted under a statistical perspective, as a measurement of the uncertainty associated with the prediction provided by each source. Ideally, all blending coefficients should equal 1, so that the SEL $L_{E,A}(d)$ provided by Eq. 10 or by Eq. 9 through Eq. 8 would be equal.

2.3.1 Estimating the blending coefficients

In order to apply the prediction method proposed in Eq. 10 for noise estimation, a preliminary design of the blending coefficients needs to be carried out. A dedicated procedure envisaged for the task will be illustrated in the following.

The starting point of the proposed procedure for coefficient computation is the processing of the ANP database. A sub-set of the aircraft therein is selected, based on similarity with respect to the target application of the prediction model. Table 2 shows the identity of the aircraft considered here. On account of the application to General Aviation, propeller-driven aircraft, the sub-set is centered on models in this category.

As pointed out, this category is of special interest for two reasons. Firstly, hybrid-electric and fully-electric propulsion are appearing in this category and type of configuration, whereas scalability to larger weights and powers is still a study topic [54]. Secondarily, aircraft in this category usually operate from Milan-Bresso airport, a test case considered for data production, as shown in the results section [45].

As explained in section 2.2.3, for each aircraft in the set, the ANP database provides a value of the global SEL at ten slant measurement distances, and for a list of power settings in departure and arrival configuration. As observed in the discussion of the validation results reported in Figure 2, the relative relevances of the noise prediction models for each source is generally different in departure and arrival. This suggests to keep the two scenarios separated, so that different blending coefficients will be estimated for departure and arrival.

An optimal approach has been selected for the practical estimation of the coefficients, based on the numerical solution of the unconstrained optimization of the following merit function

$$J = \frac{\sum_{j=1}^{10}(\overline{L_{E,A_j}} - L_{E,A_j})^2}{10} + \sum_{k=1}^{5}(x_k - 1)^2. \tag{11}$$

The term $\overline{L_{E,A_j}}$ in Eq. 11 represents the SEL obtained from the database for the j-th slant distance, whereas the term L_{E,A_j} is the result of the application of Eq. 10 to the same slant distance. The value of L_{E,A_j} is clearly a function of the choice of parameters x_k, as is the latter sum $\sum_{k=1}^{5}(x_k - 1)^2$ in the expression of J. In ideal conditions, values of $x_k = 1$, for $k = 1, \ldots, 5$. In that case, the values of $L_{E,A_j} = \overline{L_{E,A_j}}$, and both sum terms in Eq. 11 would be zero. This would yield $J = 0$ in ideal conditions, and a positive value otherwise. Therefore, the optimization problem can be configured simply as

$$\min_{(x_1,x_2,x_3,x_4,x_5)} J. \tag{12}$$

As a remark, it should be added that the elastic term represented by $\sum_{k=1}^{5}(x_k - 1)^2$ in Eq. 11 is needed to introduce the physical meaning of the blending coefficients, which represent measures of confidence in the prediction of the respective noise source models. Values of the coefficients too far from 1 (the ideal value), whilst numerically feasible, are not physically acceptable, especially in view of the generally physical acceptability of the output of each source model demonstrated for the source-bundling method (see 2.2.3). Therefore, an acceptable range for the coefficients has been arbitrarily selected between 0.5 and 1.2.

By solving the optimal problem in Eq. 12 separately for each measurement entry in the ANP database for an assigned aircraft, a set of blending coefficients valid for that aircraft is obtained for each of the entries. Considering the average and standard deviation pertaining to departure and arrival entries, the blue vertical bars relative to each aircraft displayed in Figure 3 are obtained. The amplitude of the bars refers to two times the standard deviation of the sampled data (*i.e.* 2σ). At this stage, only the coefficients pertaining to airframe, propeller and engine are investigated, due to the fact that all considered aircraft do not feature an electric component in the power-train nor a gearbox.

Looking at the vertical bars, it is clear that the information in the considered samples features much scatter. Actually, the samples are few in statistical terms. Nonetheless, in some specific cases this first result features a good coherence level, with the extreme of the attended values not exceeding the reasonable range between 0.5 and 1.2.

Of course, to obtain a more reliable estimation of the blending coefficients which is also representative of an aircraft class instead of just a single aircraft, another optimization is performed irrespective of the aircraft, *i.e.* on all entries corresponding to departure and arrival maneuvers performed by aircraft in Table 2. The result is a set of blending coefficients for departure and another set for arrival, accounting for all aircraft in the class. With such statistical sample, the results presented as horizontal bars on the plots of Figure 3 are obtained.

It can be noticed how the coefficients feature a very reduced scatter, and the 2σ range represented by the horizontal black dashed lines falls generally at a safe distance from the imposed confidence limits of 0.5 and 1.2 (axis limits on the plots). Some of the average values are actually close to 1, with a rather mild 2σ scatter. The fact that the coefficients are in average different from 1 clearly justifies the inability of the source-bundling method to correctly fit ECAC data, thus further demonstrating the potentiality of the novel source-blending method and the proposed coefficient design procedure to overcome the deficiencies of that first-guess method.

2.3.2 Validation of the source-blending method

In order to validate the source-blending method, based on the coefficients obtained as described in section 2.3.1, it is possible to perform the same kind of analysis presented in section 2.2.3.

Two rather different aircraft from the set in Table 2 are considered, namely the Cessna T206H Stationair and the Piper PA-31-350 Twin Comanche. In Figure 4 the plots for the SEL obtained from the ANP database and from the application of Eq. 10 with the optimal blending coefficients computed in section 2.3.1, and represented by the plain red lines in Figure 3, are displayed for two departure and two arrival maneuvers corresponding to different flap configurations and power settings.

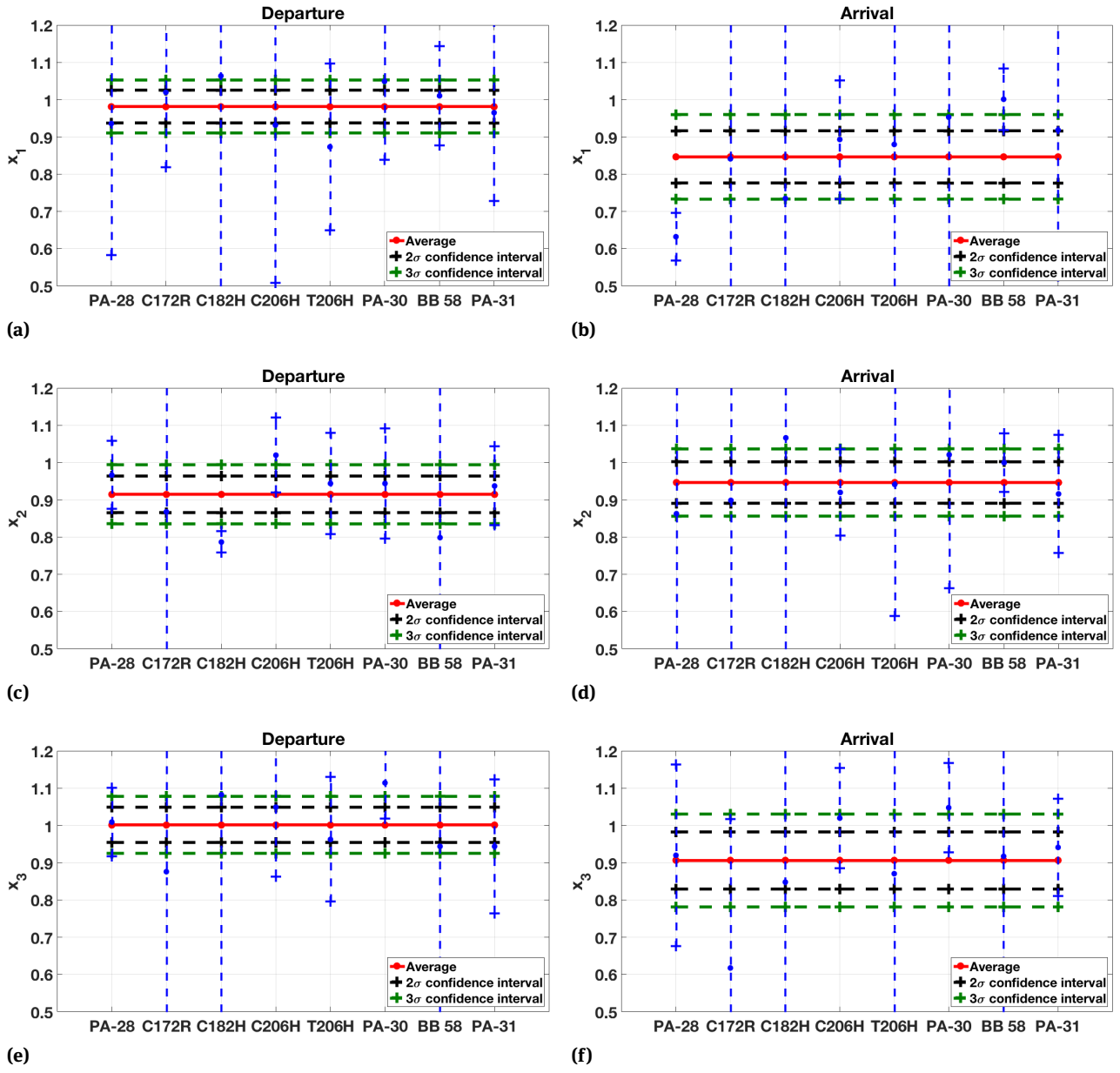

Figure 3: Statistical analysis of blending coefficients. (a,b) airframe coefficient. (c,d) propeller coefficient. (e,f) engine coefficient. (a,c,e) departure conditions. (b,d,f) arrival conditions. Blue vertical bars: results from coefficients designed considering only a specific aircraft. Horizontal bars: results obtained from coefficients designed considering all aircraft together.

Despite the 2σ confidence area contoured on the plot being relatively large when looking at the corresponding uncertainty on the noise prediction (vertical axis), the average of the estimation is remarkably close to the ANP prediction.

Similarly good results are obtained with the same values of the coefficients for the Piper PA-31-350 Twin Comanche, featuring a significantly different configuration (not reported for brevity). This is in support of the general applicability of the so-designed blending coefficients, at least when aircraft sharing the propulsion system, general configuration and weight category (rather broad) of those in the set of Table 2 are considered.

2.3.3 Blending-sources method: applicability to novel propulsion technologies

In order to check the suitability of the proposed prediction method to aircraft with novel propulsion systems, the

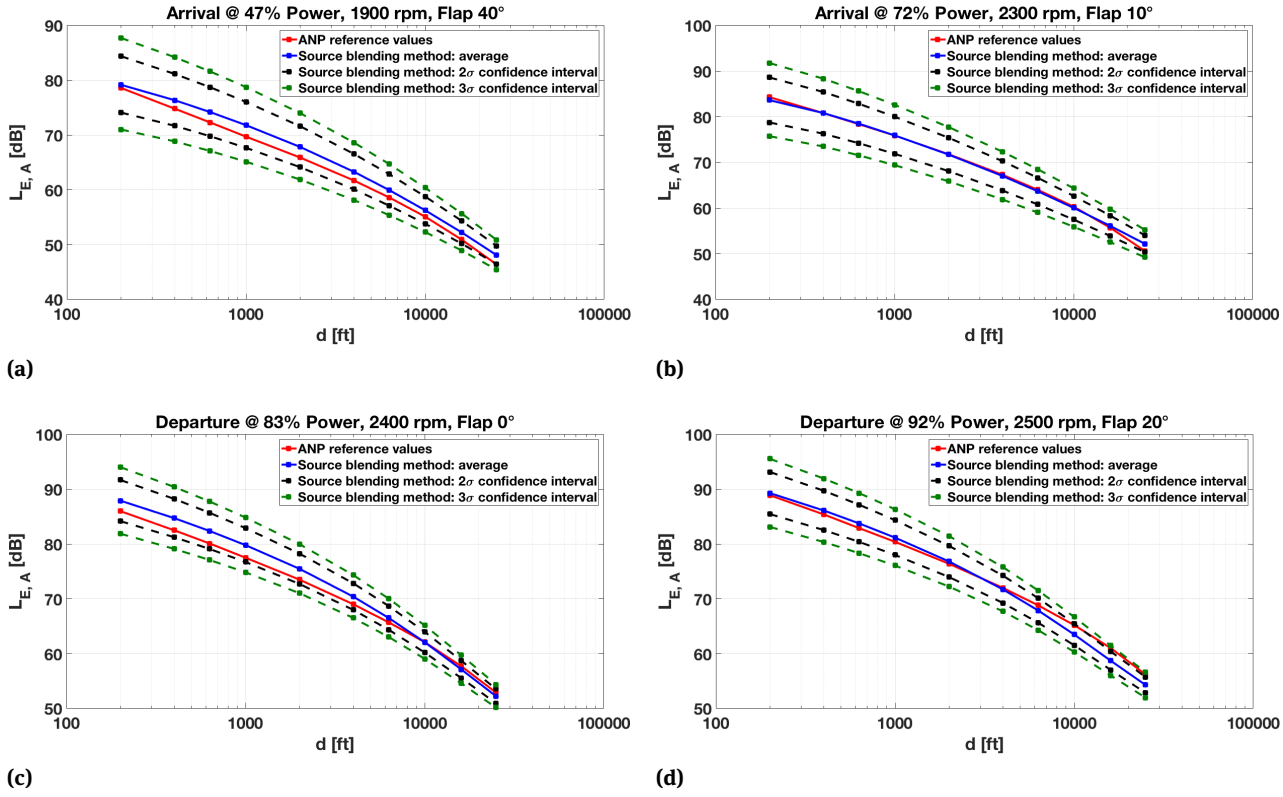

Figure 4: Comparison of SEL data from ANP database and predictions obtained from the source-blending method for a Cessna T206H. (a,b) arrival procedures. (c,d) departure procedures.

Table 3: Sound power comparison between propeller and electric motor for a Pipistrel Panthera.

Motor power/speed setting	Propeller [dB]	Electric motor [dB]	Difference [dB]
200 kW, 2 400 rpm	130.6	102.7	27.9
160 kW, 1 920 rpm	123.5	100.3	23.2
120 kW, 1 440 rpm	115.7	97.1	18.6
80 kW, 960 rpm	106.9	92.7	14.2
40 kW, 480 rpm	96.1	85.2	10.9

test case of the Pipistrel Panthera Hybrid [55] was considered. Results of an assessment for a specific practical case will be presented in the results section 3. At this stage, it is important to remark that for a hybrid-electric case more sources need to be considered than those typical to conventionally-powered aircraft (see the hypotheses in 2.3.1). In particular, the noise emission of the electric motor and of the gearbox need to be evaluated.

To better understand the following analysis, it should be noted that on the Pipistrel Panthera Hybrid, featuring a series-hybrid configuration, the propeller and the electric motor are always working in a rigidly coupled fashion. Considering the corresponding noise emissions, they will be always active together. For this reason, it makes sense to draw a comparison of the noise emitted by these sources over the operating spectrum of the power-plant.

In this view, an analysis is performed through a reasonable number of five different cases selected on the basis of the range of power and rotational speed for this kind of power-train. Power fractions of 100% to 20% every 20% have been selected. The same fractions have been applied to the rotational speed data as well, assuming a linear dependence between this quantity and power. Table 3 features a comparison of the emissions for this set of assumed values. Noise emissions for the propeller and for the electric motor are compared. Prediction values are obtained by means of the corresponding models under the five considered testing conditions.

Table 4: Sound power comparison between engine and gearbox for a Pipistrel Panthera.

Engine power/speed setting	Engine [dB]	Gearbox [dB]	Difference [dB]
115 hp, 5 800 rpm	123.0	113.3	9.7
92 hp, 5 800 rpm	123.0	112.9	10.1
69 hp, 5 220 rpm	121.2	112.3	8.9
46 hp, 3 828 rpm	115.8	111.2	4.6
23 hp, 3 828 rpm	115.8	110.0	5.8

It can be immediately inferred from Table 3 that propeller emission is always more intense than that pertaining to the electric motor, confirming an intuitive disparity between these two sources. The minimum difference is higher than 10.9 dB, with a peak value of 27.9 dB for the condition corresponding to the most intense emission.

In a totally similar fashion, the emission of the piston engine, acting as a power generation systems on board the Pipistrel Panthera Hybrid, can be compared to that of the gearbox. As these two sources always act in a rigidly coordinated fashion, it makes sense to evaluate the corresponding noise emissions. The same power fractions previously considered for obtaining the values in Table 3 are scaled to the maximum power of the internal combustion engine, while the corresponding rotational speed fractions are obtained from the database by Yacovitch [51], since differently from the case of the electric motor a linear dependence of power to rotational speed cannot be safely assumed. On Table 4 the noise emissions in terms of sound power for the engine and gearbox are reported for these five conditions, used as a reference when internal combustion engine is activated.

In Table 4 it can be noted that, as the model assumed for engine noise is not a function of the actual power output, but of the rotational speed only, when the rotational speed is the same the noise emitted by the engine does not change. On the other hand, the noise produced by the gearbox is a function of both power and rotational speed.

Again, the engine always prevails in terms of emitted noise on the gearbox. The difference between the output of these sources is at least 4.6 dB, with a peak of 10.1 dB.

Based on this analysis, the electric motor and gearbox can be ruled out for the case of the hybrid-electric Pipistrel Panthera Hybrid on account of their negligible noise contribution. Furthermore, considering the conventional configuration and weight of the Pipistrel Panthera in both its hybrid-electric and conventional versions, fitting well in the database of Table 2, this in turn enables the application of the source-blending method based on the sole coefficients already designed (see 2.3.1) also to this aircraft model.

3 Example noise emission analyses

Once its accuracy level has been assessed through validations, the proposed source-blending prediction method can be deployed to analyze cases of practical interest, in particular investigating the potential of hybrid-electric and fully-electric propulsion in mitigating noise pollution around airports.

The airport of Milan-Bresso (ICAO: LIMB) has been selected as a test case for quantitative analyses presented herein. This airport is the home base of the Aero Club Milano fleet, which is operated for instructional purposes and for pleasure flights. The fleet is mainly composed of Cessna C172 in several variants, and Piper models including both single-propeller and twin-propeller aircraft. The airport features a single 1 080x30 m asphalt runway with a 18/36 alignment, and an elevation of 484 ft above sea level. Geographically located at the northern border of the municipal area of Milan, Milan-Bresso is completely surrounded by densely populated districts of the greater Milan area. This feature makes it noise-emission-critical, and has fueled an interest for the present analysis.

Based on a realistic description of the circuit around the runway of Milan-Bresso, two analyses will be proposed in the present section. At first, an assessment of the effect on the noise levels perceived on ground when parts of the circuit (or even all of them) are flown in electric mode will be described in detail. To this aim, it will be hypothesized to fly a typical circuit by means of two different conventionally powered aircraft, *i.e.* not provided with electric components in the power-plant in reality. Several cases will be analyzed where the piston engine(s) is conditionally activated in some clearly identified legs of the circuit. In so doing, as no re-design of the aircraft is taking place, it is implicitly assumed that the necessary battery pack and hybrid-electric power-plant (or even a fully-electric power-plant, in case all the circuit is completely flown without recurring to a piston engine) can be put on board the aircraft without altering its take-off weight and power requirement. That said, this comparative analysis produces valuable re-

Table 5: Characteristics of the grid for the ground track of the circuit in Figure 5.

Leg	Length (on ground) [ft]	Number of sensors	Resolution [ft]
Departure	8 990	24	391
Crosswind	4 360	9	545
Downwind	15 660	21	783
Base	4 370	9	546
Final	6 670	18	392

sults to better understand in what parts of the circuit electric propulsion (*i.e.* the deactivation of piston engines on hybrid-electric power-trains) may have a greater impact in terms of noise pollution.

Secondarily, a comparison is attempted between three existing aircraft, including a Pipistrel Panthera Hybrid, for an assigned circuit trajectory and given an activation/deactivation strategy for the power generation system (*i.e.* the piston engine on-board this aircraft). This produces very reasonable results, which highlight the quantitative advantage that would correspond to a fleet switching from aging conventionally powered aircraft towards an existing hybrid-electric aircraft, sharing the weight category and a similar mission profile.

3.1 Studying the effect of power-train operational mode

The ECAC modeling approach recalled in section 2.1.1 is applied to the discretization of the right-hand circuit of RWY18, most commonly in use in normal operation around Milan-Bresso. The circuit as typically flown by a Cessna 172R aircraft is presented on Figure 5(a), and features a downwind leg at an altitude of 1 500 ft QNH. It should be recalled that the discretization is not only geometrical, but also applied to flight mechanics parameters, as specified by ECAC guidelines.

The same two aircraft models already introduced in section 2.3.2, namely a Cessna T206H Stationair and Piper PA-31-350 Navajo Chieftain, are considered as test-beds.

The prediction of noise emissions is carried out by computing the SEL on an assigned grid of sensors on ground. The source-blending method, with the coefficients computed in section 2.3.1 can be applied for both aircraft, with the flight trajectory and flight mechanics parameters along the circuit assigned as input.

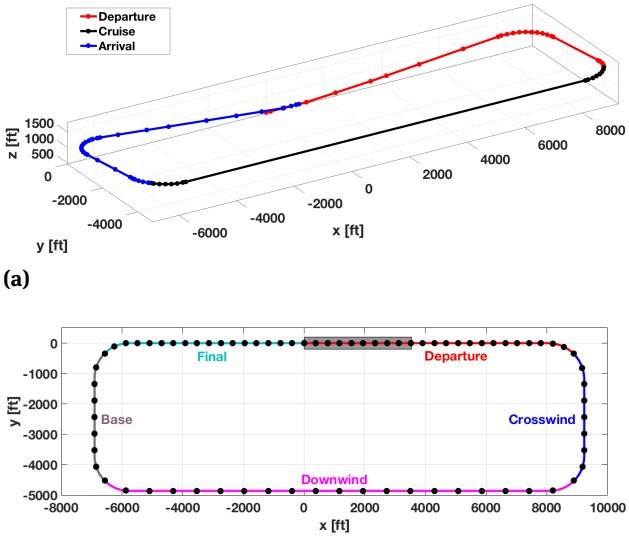

Figure 5: Geometry discretization (a) and noise sensor placement (b) of the RWY18 right-hand circuit of Milan-Bresso.

3.1.1 Sound exposure along the circuit ground track

In a first stage, a grid of sensors is designed along the ground trace of the circuit. On Figure 5(b) the adopted map of sensor points is displayed. The plot also highlights the extension of the five legs in the circuit - namely departure, crosswind, downwind, base and final.

The positioning of the grid follows the guidelines of ECAC validation scenarios [47]. As typical, the discretization is the result of a compromise between accuracy and computational cost, defined by means of a convergence analysis on the results. In Table 5 are reported basic geometrical data of the grid.

Clearly, the legs where altitude is changing more quickly (departure and final) correspond to a finer discretization, whereas the downwind leg, where the aircraft is flying at constant altitude, is associated to a loose discretization. The total number of sensors at this stage is 76. It is also worth mentioning that no transient is considered in the adopted noise emission models, so all changes in

Table 6: Piston engine conditional activation cases.

ID	Circuit legs with piston engine activated
1	All
2	Departure, Crosswind
3	Departure, Crosswind, Downwind
4	Downwind
5	Downwind, Base, Final
6	Base, Final
7	None

input and output variables involved in those models (*e.g.* power settings, rotational speed of the propeller, etc.) take place instantaneously.

As explained in the introduction to section 3, different power management strategies for flying the circuit are considered. Besides the extreme cases represented by using only the piston engine(s) (conventional propulsion case) or the electric motor (fully-electric case), five further intermediate cases are investigated, listed in Table 6. In order to present the results of the analysis in a concise form, as looking at the sensors one by one would be impractical, a more comprehensive measure is introduced. On account of the energetic nature of the SEL measurement, an energy-based spacial average $\overline{L_E}$ for an arbitrary piece of the ground track trajectory is computed based on the expression

$$\overline{L_E} = 10 \log_{10} \left(\frac{\int_{s_1}^{s_2} 10^{\frac{L_E(s)}{10}} \mathrm{d}s}{s_2 - s_1} \right) \tag{13}$$

where the SEL $L_E(s)$ is expressed as a function of the position along a segment of the ground track of the circuit, and s_1 and s_2 correspond to the initial and final extremes of that segment respectively. By adopting the measurement in Eq. 13 and applying it to each leg under the circuit (see Figure 5(b)), it is possible to obtain the results in Table 7 and Table 8, respectively for the Cessna T206H and for the Piper PA-31-350. Both tables display the results of the application of conditional activation strategies for the piston engine listed in Table 6.

At a glance, a comparison of Table 7 and 8 highlights a generally higher noise for the latter, corresponding to the Piper aircraft. This is the result of a larger take-off weight, fuselage size, wing and tail area, landing gear front section, and of a twin-engined configuration, as opposed to smaller size and single-engined configuration of the Cessna aircraft.

Comparing the legs to one another, it is possible to see that the noise exposure quotas pertaining to departure and final are the highest. For departure, this is the result of a combination of low distance from ground and high power settings. As for the sensors under the final leg, these are exposed to high noise from departure, which justifies the high values of this part (this will be evident on sound exposure maps in the next subsection).

Considering only the extreme piston engine deactivation strategies, *i.e.* cases 1 and 7 in Table 6, it is possible to realize that the sensors under the crosswind leg are associated to SEL values immediately below those pertaining to departure and final, as a result of intermediate power settings and altitudes. Downwind and base are associated to the lowest SEL values, due to a higher distance from ground and lower power settings.

Analyzing the results in terms of conditional activation strategies, it is apparent that the all-electric (case 7) and all piston powered (case 1) scenarios are associated to the lowest and highest SEL values respectively. Looking at the intermediate cases, it can be seen that SEL values for each leg are roughly polarized around two extreme values. This means that when a leg is flown with the piston engine working, SEL values under that leg assume roughly an extreme, whereas when the piston engine is deactivated, the SEL values are always close to the opposite extreme. Polarization is further confirmed by the similarity between the SEL measures averaged over all legs for the cases 4, 5, 6 and 7, *i.e.* when the piston engine is not run or it is run only at low power (*i.e.* on downwind, base and final).

3.1.2 Sound exposure over airport area and surroundings

To complement the analysis along the ground track of the circuit, a less refined grid of sensors has been adopted to quantify the SEL on the ground over a more extensive geometrical area. Referring to Figure 5(b), the new sensor grid extends between -15 000 ft and 15 000 ft in the direction of the runway centerline, and from -10 000 ft to 5 000 ft in the cross-centerline direction. The resolution is 1 000 ft in both directions, yielding a total of 496 sensors, which allows to keep computational time reasonably low [1].

The SEL contour lines associated to the extreme cases in Table 6 are reported in Figure 6 for the case of both aircraft under investigation.

1 With this discretization, computational time for one of the plots in Figure 6, *i.e.* over the whole grid, is typically between 75 and 90 minutes for the PA-31 and the T206H respectively on a single dual-core `Intel Core i5` processor.

Table 7: Average SEL for the Cessna T206H Stationair. Results for conditional activation cases listed in Table 6.

ID	Departure [dB]	Crosswind [dB]	Downwind [dB]	Base [dB]	Final [dB]	All legs [dB]
1	93.18	83.22	78.82	76.22	88.92	88.15
2	93.15	83.02	76.44	74.39	88.68	87.99
3	93.16	83.22	78.79	74.82	88.69	88.08
4	90.22	80.45	78.48	74.79	86.21	85.43
5	90.26	80.45	78.52	76.20	86.62	85.55
6	90.26	80.06	75.97	75.89	86.61	85.38
7	90.22	80.06	75.91	74.36	86.20	85.25

Table 8: Average SEL for the Piper PA-31-350 Navajo Chieftain. Results for conditional activation cases listed in Table 6.

ID	Departure [dB]	Crosswind [dB]	Downwind [dB]	Base [dB]	Final [dB]	All legs [dB]
1	97.25	87.83	83.19	80.30	91.72	92.03
2	97.22	87.69	80.66	78.66	91.33	91.83
3	97.22	87.83	83.17	78.99	91.34	91.94
4	93.68	85.01	82.96	78.97	88.84	88.87
5	93.75	85.01	82.99	80.29	89.49	89.05
6	93.75	84.73	80.34	80.04	89.47	88.83
7	93.67	84.73	80.29	78.64	88.82	88.65

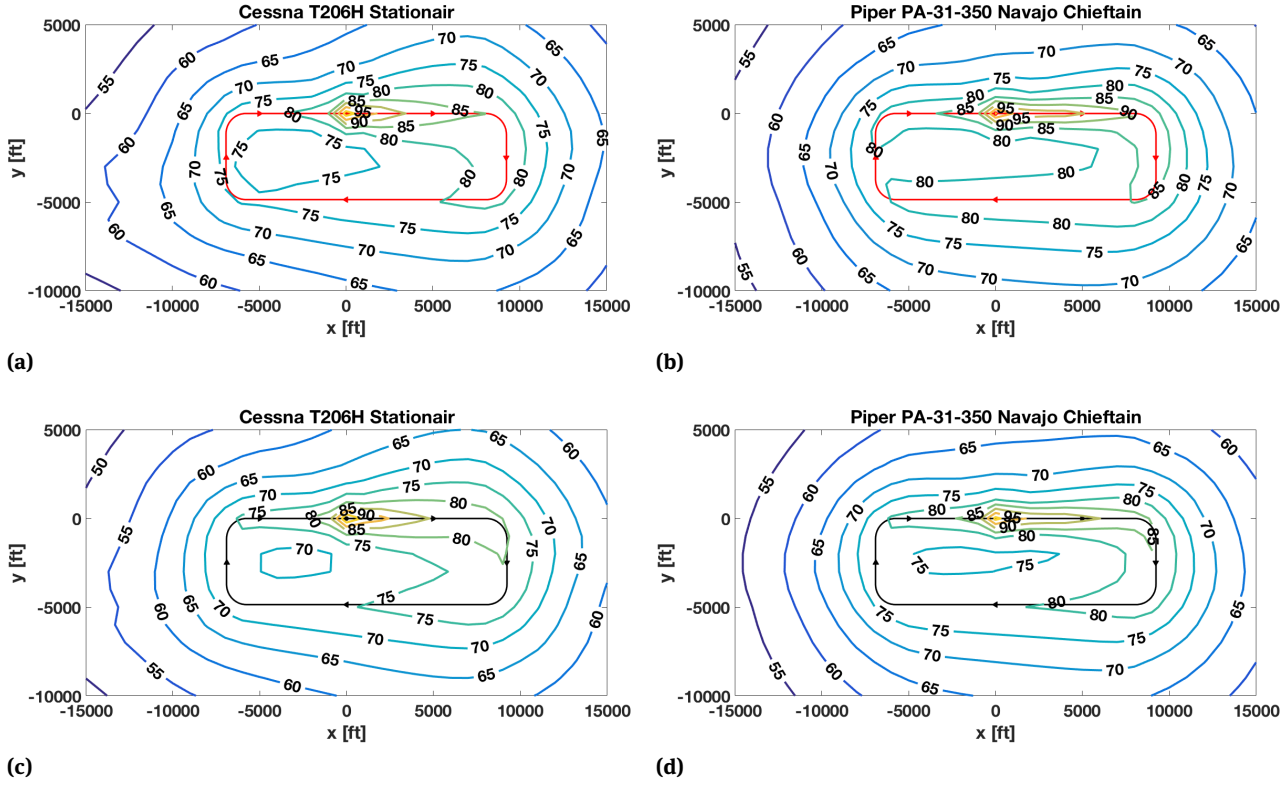

Figure 6: Contour plots of SEL over an extended sensor grid around Milan-Bresso airport. (a,b) case 1 (piston engine always active), (c,d) case 7 (piston engine always deactivated), as per Table 6. (a,c) Cessna T206H Stationair. (b,d) Piper PA-31-350 Navajo Chieftain. Values in dB.

Table 9: SEL contoured areas for Cessna T206H Stationair. Case ID corresponding to Table 6.

ID	A_{70} [ft^2]	A_{75} [ft^2]	A_{80} [ft^2]	A_{85} [ft^2]	A_{90} [ft^2]	A_{95} [ft^2]	A_{100} [ft^2]
1	$2.1 \cdot 10^8$	$1.2 \cdot 10^8$	$4.4 \cdot 10^7$	$9.8 \cdot 10^6$	$2.8 \cdot 10^6$	$7.4 \cdot 10^5$	$8.8 \cdot 10^4$
2	$1.8 \cdot 10^8$	$8.9 \cdot 10^7$	$3.8 \cdot 10^7$	$9.6 \cdot 10^6$	$2.7 \cdot 10^6$	$7.2 \cdot 10^5$	$8.4 \cdot 10^4$
3	$2.0 \cdot 10^8$	$1.1 \cdot 10^8$	$4.3 \cdot 10^7$	$9.7 \cdot 10^6$	$2.7 \cdot 10^6$	$7.2 \cdot 10^5$	$8.5 \cdot 10^4$
4	$1.8 \cdot 10^8$	$9.4 \cdot 10^7$	$2.4 \cdot 10^7$	$4.7 \cdot 10^6$	$1.4 \cdot 10^6$	$2.6 \cdot 10^5$	
5	$1.9 \cdot 10^8$	$1.0 \cdot 10^8$	$2.5 \cdot 10^7$	$4.7 \cdot 10^6$	$1.4 \cdot 10^6$	$2.7 \cdot 10^5$	
6	$1.7 \cdot 10^8$	$7.6 \cdot 10^7$	$2.1 \cdot 10^7$	$4.7 \cdot 10^6$	$1.4 \cdot 10^6$	$2.7 \cdot 10^5$	
7	$1.6 \cdot 10^8$	$7.0 \cdot 10^7$	$2.0 \cdot 10^7$	$4.6 \cdot 10^6$	$1.4 \cdot 10^6$	$2.5 \cdot 10^5$	

Table 10: SEL contoured areas for Piper PA-31-350 Navajo Chieftain. Case ID corresponding to Table 6.

ID	A_{70} [ft^2]	A_{75} [ft^2]	A_{80} [ft^2]	A_{85} [ft^2]	A_{90} [ft^2]	A_{95} [ft^2]	A_{100} [ft^2]	A_{105} [ft^2]
1	$2.6 \cdot 10^8$	$1.8 \cdot 10^8$	$9.4 \cdot 10^7$	$2.6 \cdot 10^7$	$7.8 \cdot 10^6$	$2.4 \cdot 10^6$	$3.2 \cdot 10^5$	$3.6 \cdot 10^2$
2	$2.3 \cdot 10^8$	$1.6 \cdot 10^8$	$6.0 \cdot 10^7$	$2.4 \cdot 10^7$	$7.7 \cdot 10^6$	$2.3 \cdot 10^6$	$3.0 \cdot 10^5$	$1.9 \cdot 10^2$
3	$2.5 \cdot 10^8$	$1.7 \cdot 10^8$	$8.8 \cdot 10^7$	$2.6 \cdot 10^7$	$7.7 \cdot 10^6$	$2.4 \cdot 10^6$	$3.0 \cdot 10^5$	$2.0 \cdot 10^2$
4	$2.3 \cdot 10^8$	$1.6 \cdot 10^8$	$7.4 \cdot 10^7$	$1.3 \cdot 10^7$	$3.7 \cdot 10^6$	$6.1 \cdot 10^5$	$3.2 \cdot 10^4$	
5	$2.4 \cdot 10^8$	$1.7 \cdot 10^8$	$7.9 \cdot 10^7$	$1.4 \cdot 10^7$	$3.8 \cdot 10^6$	$6.6 \cdot 10^5$	$3.8 \cdot 10^4$	
6	$2.1 \cdot 10^8$	$1.4 \cdot 10^8$	$4.9 \cdot 10^7$	$1.3 \cdot 10^7$	$3.8 \cdot 10^6$	$6.6 \cdot 10^5$	$3.7 \cdot 10^4$	
7	$2.1 \cdot 10^8$	$1.4 \cdot 10^8$	$4.5 \cdot 10^7$	$1.2 \cdot 10^7$	$3.7 \cdot 10^6$	$6.1 \cdot 10^5$	$3.2 \cdot 10^4$	

In order to provide a quantitative description of the noise footprint, Table 9 and 10 display the areas A_{nl} contoured by a line corresponding to a given noise level nl (in dB).

From Table 9, in cases 1, 2 and 3, where the piston engine is working in the departure and crosswind legs, *i.e.* correspondingly at higher regimes, it can be observed the appearance of a core of higher noise intensity, which especially from Figure 6(a) can be spotted along the ground track of the circuit, and in particular along the departure leg.

Comparing the cases from 1 to 3 to the set from 4 to 7, from Table 9 it can be noticed that lower area values are associated to all noise levels for the four latter cases, and the core associated to the highest noise disappears in the same activation scenarios. This is in support of the results presented with a more limited analysis in section 3.1.1, and is confirmed graphically on the plot in Figure 6(c).

The outcome of the analysis for the twin-engined Piper model is qualitatively similar to that for the Cessna single-engined aircraft. As observed, the configuration of this Piper model is forcibly associated to higher noise emissions than the Cessna aircraft. This is testified by the appearance of a top noise core associated to 105 dB in Table 10, whereas the corresponding value in Table 9 is associated to 100 dB.

The generally more intense noise emission of the Piper is testified also by the larger areas corresponding to the same SEL level, as can be seen from the comparison of corresponding columns on Table 9 and 10. This has a match in the stretched shapes of contoured areas associated to the highest noise levels in the (b) and (d) plots of Figure 6, pertaining to the Piper aircraft. By comparison, the contoured areas associated to the highest noise levels for the Cessna ((a) and (c) plots) are clearly more compact.

3.2 Studying the effects of different propulsion systems

As reported in the introductory part of section 3, after assessing the effect of different piston engine activation strategies, without altering the actual structure of two existing conventionally-powered aircraft, an analysis is attempted on three more realistic test-beds.

Three aircraft are selected for the purpose, namely a Cessna C172R Skyhawk, a Pipistrel Panthera with conventional propulsion, and its novel hybrid version, the Pipistrel Panthera Hybrid.

Again, the case of the RWY18 right-hand circuit of Milan-Bresso airport has been considered. As pointed out, the computation of sound exposure is based on the definition of a segmented aircraft trajectory and on the creation of a set of NPD data, made according to the source-blending method. The behavior of the flight mechanics parameters along the trajectory of the circuit has been simu-

lated following the guidelines of the ANP database, starting from the data listed for a Cessna C172R. The guidelines have been emended considering the actual circuit altitude of the considered circuit.

For the case of the Pipistrel Panthera in both its configurations, not included in the database, the same trajectory of the Cessna C172R has been assumed. Due to a general similarity in size, weight and power, this assumption has not been deemed dramatically heavy or dangerous. The aforementioned altitude limitations due to regulations over Milan-Bresso further reduce the impact of such assumption - actually, all aircraft operating from this airport fly a very similar circuital trajectory. It also brings in as a plus the chance to assess differences in emissions only due to aircraft-specific features, and not to differences between trajectories.

Concerning noise emissions, the blending coefficients introduced and designed in section 2.3 have been adopted for all aircraft. For the case of the Panthera Hybrid, propelled by a series-hybrid group, it has been hypothesized that the propeller is always driven by the brushless Siemens e-Motor SP150D. The power trend with respect to rotational speed is assumed linear, so that power is directly proportional to rotational speed.

In order to keep as close as possible to a realistic scenario, the Panthera Hybrid circuit flight has been analyzed assuming to activate the piston engine, a Rotax 914 [56], only when the aircraft reaches the maximum allowable altitude, as operationally prescribed. In turn, this roughly corresponds to an engine activation along the downwind leg. Clearly, the two conventionally powered aircraft are analyzed with the piston engine always running.

The contour plots of the SEL, computed on the same grid considered in section 3.1.2, are presented in Figure 7.

As pointed out, from the three plots in Figure 7 it can be noted that the most intense SEL values are recorded in proximity to the departure leg, as this is characterized by the highest power settings and the lowest slant distances between the aircraft and the receiver on ground. The higher intensity of emissions in this phase is also responsible for relatively high SEL values on the ground track of the final leg. By comparison, the higher distance from ground typical of the downwind leg, and the lower power settings of the base and final (the latter with the caveat just mentioned), are associated to a generally lower noise mark on ground for these legs.

Comparing the plots pertaining to the two conventional aircraft, these are qualitatively similar, but a difference in the extreme values can be noticed far from the circuit, especially port of the aircraft along the downwind leg, showing a generally lower noise footprint for the Panthera.

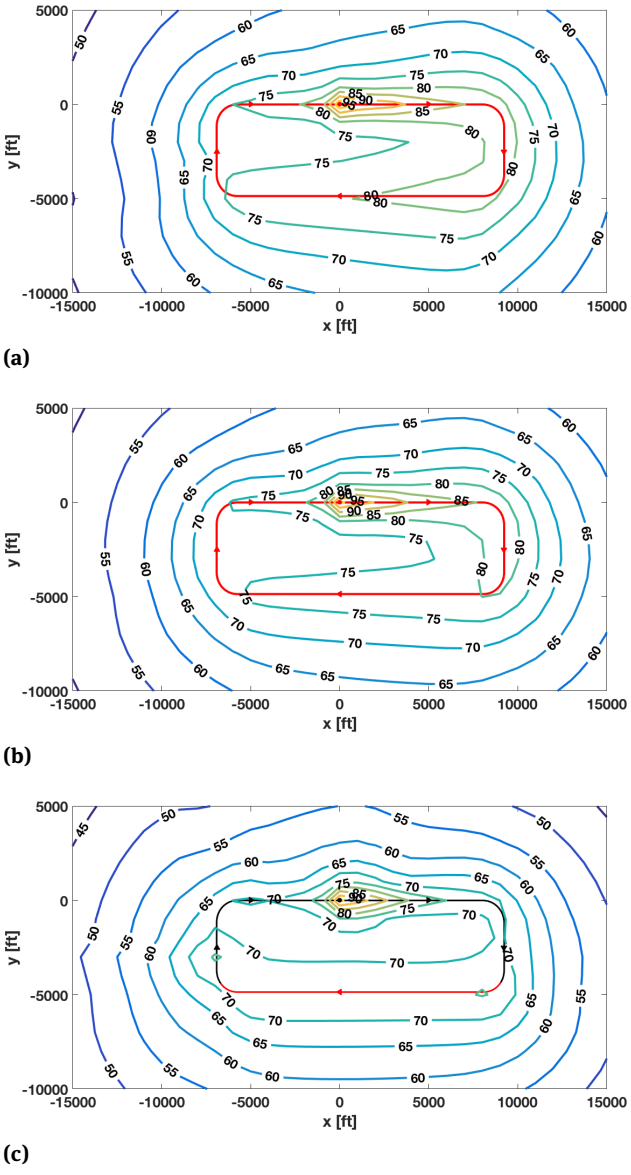

Figure 7: Contour plots of SEL, same grid as Figure 6. (a) Cessna C172R Skyhawk. (b) Pipistrel Panthera. (c) Pipistrel Panthera Hybrid.

Inside the circuit (*i.e.* in the immediate vicinity of the runway and aerodrome area) more significant differences can be appreciated in the shapes of the contour plots, but the values of the SEL are generally similar for both aircraft.

The Panthera Hybrid case displays some marked differences with the other two cases. Looking at the regions out of the circuit, the SEL is generally significantly lower for the hybrid aircraft, especially closer to high-power legs (departure, crosswind). It can be noticed also that the SEL gradient along the departure leg is more pronounced for the hybrid case. Looking at the downwind leg, the activation of the piston engine at maximum regime in this phase produces a 70 dB contour line parallel to the downwind

Table 11: SEL contoured areas for the three aircraft under analysis in section 3.2. Data corresponding to the plots in Figure 7.

Aircraft	A_{70} [ft^2]	A_{75} [ft^2]	A_{80} [ft^2]	A_{85} [ft^2]	A_{90} [ft^2]	A_{95} [ft^2]	A_{100} [ft^2]
Cessna C172R	$1.9 \cdot 10^8$	$1.1 \cdot 10^8$	$3.4 \cdot 10^7$	$6.2 \cdot 10^6$	$1.9 \cdot 10^6$	$2.5 \cdot 10^5$	
Pipistrel Panthera (conventional)	$1.8 \cdot 10^8$	$9.0 \cdot 10^7$	$2.8 \cdot 10^7$	$7.4 \cdot 10^6$	$2.6 \cdot 10^6$	$6.0 \cdot 10^5$	$1.6 \cdot 10^4$
Pipistrel Panthera Hybrid	$7.9 \cdot 10^7$	$8.3 \cdot 10^6$	$4.1 \cdot 10^6$	$1.9 \cdot 10^6$	$5.5 \cdot 10^5$	$9.0 \cdot 10^3$	

leg, which contrasts with the noise intensity decay registered for the two conventional airplanes.

To quantitatively compare the results in Figure 7, the same approach adopted for Table 9 and 10 has been adopted in Table 11 for the three aircraft considered in this phase.

Considering in a first stage the two conventionally-propelled models, it can be noticed that, somewhat unexpectedly, sound exposures higher than 100 dB are produced by the conventional Panthera, which is also associated to the largest contoured areas for SEL values of 85 dB and above, *i.e.* performing somewhat worse than the older C172R. Looking at the emission maps in Figure 7, such effect is likely due to the take-off phase, as exposures higher than 85 dB are registered only near the departure leg. A possible explanation for this effect is linked to Dobrzynski's model for piston engine noise [12], which accounts only for maximum power and not for its actual value. The conventional Panthera version is equipped with a 260-hp Lycoming IO-540-V, which is much more powerful than the Lycoming IO-360-L2A [57] on the Cessna C172R Skyhawk. This results into a generally higher engine noise, and consequently also a larger exposure for the conventional Panthera during take-off and climb, *i.e.* two phases in which the contribution of the engine is mostly relevant.

On the other hand, the areas relative to the lower SEL values are higher for the Cessna C172R Skyhawk than the conventional Panthera (*e.g.* the 80 dB and the 75 dB lines). Looking at the emission maps in Figure 7, this difference is associated with a different behavior in the first part of the downwind leg, and may be related to the landing gear contribution to the overall aircraft noise. As engine power is not at its maximum value over this leg, the engine and propeller noise emission levels are comparable to the airframe contribution, in turn mainly related to landing gear, greater than wing noise level and for a flap deflection assumed null. Considering the Panthera, landing gear retraction has been assumed in the generation of the NPD data adopted for this flight phase, whereas the Cessna C172R Skyhawk is equipped with a fixed landing gear, contributing to the difference in overall aircraft noise.

Focusing now on the Panthera Hybrid, the lower contoured areas in Table 11 confirm the generally lower noise footprint of this aircraft, as observed. There are also in this case locations where SEL reaches 95 dB, but the corresponding contoured area is two orders of magnitude smaller than the value pertaining to the Cessna C172R Skyhawk and conventional Pipistrel Panthera. The region contoured by the 90 dB and the 85 dB contour lines is three-times smaller for the Panthera Hybrid with respect to Cessna C172R Skyhawk, as a result of the different gradient in proximity to the departure leg, as observed. The area enclosed by the 85 dB line for the Panthera Hybrid roughly matches that associated to the 90 dB level for the Cessna C172R Skyhawk.

Considering the lowest exposure levels, a more interesting comparison is made with respect to the conventional Panthera, associated to lower values than the Cessna C172R Skyhawk. Looking at the 75 dB and 80 dB levels, the corresponding enclosed region is one order of magnitude larger for the conventional Panthera than for its hybrid-electric version. Since the aerodynamic and structural characteristics are the same for the two aircraft, such behavior is due to the effect of the electric component of the power-train.

On the other hand, the area contoured by the 70 dB contour line for the case of the Panthera Hybrid is only 2.2 times smaller than the corresponding value for the conventional version, as a result of the large 70 dB area produced on both sides of the downwind leg, as noted in Figure 7(c).

4 Conclusions

The present paper is focused on the setup of a practical procedure to predict the noise produced and propagated by an aircraft featuring a novel hybrid-electric or fully-electric power-train.

To achieve this goal, the following step-by-step conceptual and practical procedure has been followed and presented.

- A reference noise prediction model has been built and validated, according to the existing standard for conventionally propelled aircraft. Such prediction model computes the noise distribution on ground,

considering the aircraft as a single noise source. Validation is carried out in a scenario (*i.e.* airfield, trajectory and aircraft) assigned by regulations.

– In order to prepare a new prediction model applicable to aircraft featuring a novel hybrid-electric or fully-electric propulsion system, five different noise sources on board the aircraft are considered - namely airframe (with sub-components), propeller, engine, electric motor and gearbox. In order to combine the models for each sub-component, some manipulation is necessary, to obtain as output from each of them a measure of the same physical quantity. By accounting for these specific sources, the scope is reduced to propeller-driven aircraft, typically designed in the General Aviation (GA) category. Nonetheless, with a different choice of noise components, the procedure can be conceptually extended to other types of aircraft. Of course, the presence of a gearbox and electric motor among the noise sources allows to apply the ensuing procedure to hybrid-electric or fully-electric power-trains.
– A superimposition of the sources is attempted in the source-bundling method. A validation is carried out considering conventionally propelled aircraft operating from an existing airfield (Milan-Bresso) and accounting for a detailed description of their respective circuital trajectories. The result highlights a low global accuracy on the prediction of the sound exposure level (SEL) due to the whole aircraft, but reasonably realistic results considering the sources one by one.
– A novel source combination method is introduced, named source-blending method, where the output of each source is blended with all others in an optimal fashion, to bear the overall noise prediction obtained from the reference method proposed by regulations (first point in the list). The optimal blending coefficients are designed considering a pool of reference aircraft, for which both the overall noise produced and the quotas pertaining to each source can be evaluated. This yields a proportion to be applied to the measurements from each sub-source to correctly produce the noise pertaining to the whole aircraft through a proper combination (blending). The applicability of the same proportion (same blending coefficients) to many aircraft in a class is demonstrated. As a side product of the design procedure yielding the coefficients, the electric motor and gearbox are ruled out as insignificant sources of noise, due to their very low contribution compared to the other sources, for the considered class of aircraft.
– The source-blending method is applied to two analyses of practical interest, both prepared considering the realistic case of the circuit around Milan-Bresso airfield. In a first instance, the effect of different activation strategies of the fuel-burning power generation system is considered, showing the effectiveness of some of them in reducing the noise perceived on ground by a significant amount. In this analysis, ideal hybridized versions of two existing aircraft have been adopted for testing. In the second scenario, a comparison is carried out between existing conventionally propelled aircraft and the Pipistrel Panthera Hybrid, as of today among the few manufactured hybrid-electric aircraft. The potential of the hybrid-electric architecture is fully demonstrated in terms of noise reduction, thus quantitatively showing the gain offered by this novel type of power-train, and confirming through reasonable results the ability of the proposed noise estimation method.

At the current level of maturity of the hybrid-electric and fully-electric technologies for aviation power-trains, it has been preferred to put an accent on the GA category, obtaining more readily applicable results. As a development of the present research, a way to extend this prediction methodology to larger aircraft will be investigated. The lack of consolidated data from existing prototypes in higher weight categories makes the task very demanding. Yet providing prospective results assessing the advantages of further application of this novel technology would allow to quantify potential gains at an aircraft design level, in turn likely contributing to the optimal design of larger hybrid-electric or fully-electric aircraft in the future.

Conflict of Interests: The authors declare no conflict of interests regarding the publication of this paper.

Acknowledgement: This research was partly funded by the EU Horizon 2020 research and innovation program, under grant agreement N. 723368.

References

[1] EUROCONTROL, The Aircraft Noise and Performance (ANP) database: an internationl data resource for noise modellers, 2006.
[2] ECAC, Report on standard method for computing noise contours around civil airports – Volume 2: Technical Guide. Neuilly-sur-Seine, France, 2016.
[3] ICAO, Recommended method for computing noise contours around airports. Montreal, QC, 2008.

[4] Ollerhead J.B., Rhodes D.P., Viinikainen M.S., Monkman D.J., Woodley A.C., The UK civil aircraft noise contour model ANCON: Improvements in Version 2., Tech. Rep. 9842, NATS, 1999.
[5] Pietrzko S., Bütikofer R., FLULA – Swiss aircraft noise prediction program, in Proceedings of Acoustics 2002 Innovation in Acoustic and Vibration, (Adelaide, Australia), November 13-15, 2002.
[6] Isermann U., Matschat K., Müller E.A., Prediction of aircraft noise around airports by a simulation procedure, Proc. Inter-Noise 86, (Cambridge, MA), July 21-23, 1986, 717-722.
[7] Deutsche Umweltbundesamt, Anleitung zur Berechnung von Larmschutzbereichen (AzB), 2007.
[8] Malbequi P., Rozenberg Y., Bulte J., Aircraft noise prediction in the IESTA program, Proc. 3rd European Conference for Aerospace Sciences (EUCASS 2009), (Versailles, France), July 6-9, 2009.
[9] EUROCONTROL, IMPACT: EUROCONTROL's integrated aircraft noise and fuel burn & emission modelling platform, 2016.
[10] United States Department of Transportation, Aviation Environmental Design Tool (AEDT) – Version 2d – User guide, 2017.
[11] Lopes L.V., Burkley C.L., Design of the next generation aircraft noise prediction program: ANOPP2, Proc. 17th AIAA/CEAS Aeroacoustic Conference, (Portland, OR), June 5-8, 2011.
[12] Bertsch L., Dobrzynski W., Guerin S., Tool development for low-noise aircraft design, J. Aircraft, 2010, 47(2), 694-699.
[13] Farassat F., Succi G.P., A review of propeller discrete frequency noise prediction technology with emphasis on two current methods for time domain calculations, J. Sound Vibr., 1980, 71(3), 399-419.
[14] Curle N., The influence of solid boundaries upon aerodynamic sound, Proc. Royal Soc. A, 1955, 231(1187), 505-514.
[15] Chase D.M., Sound radiated by turbulent flow off a rigid half-plane as obtained from a wave vector spectrum of hydrodynamic pressure, J. Acoust. Soc. Amer., 1972, 52(3B), 1011-1023.
[16] Hanson D.B., Shielding of prop-fan cabin noise by the fuselage boundary layer, J. Sound Vibr., 1984, 92(4), 591-598.
[17] Hanson D.B., Parzych D.J., Theory for noise of propellers in angular inflow with parametric studies and experimental verification, Contractor report CR-4499, NASA, 1993.
[18] SAE Aerospace, Prediction procedure for near-field and far-field propeller noise - AIR 1407, 1977.
[19] Rathgeber R.K., The development of a flyover noise prediction technique using multiple linear regression analysis, SAE Technical Paper Series, 810588, 1981.
[20] Royal Aeronautical Society, Prediction of near-field and far-field harmonic noise from subsonic propellers with non-axial inflow - ESDU 11005, 2011.
[21] Fink M.R., Noise component method for airframe noise, J. Aircraft, 1979, 16(10), 659-665.
[22] Munson A.G., A modeling approach to nonpropulsive noise, Proc. 3rd AIAA Aeroacoustics Conference, (Palo Alto, CA), July 20-23, 1976.
[23] Amiet R.K., Noise due to turbulent flow past a trailing edge, J. Sound Vibr., 1976, 47(3), 387-393.
[24] Howe M.S., A review of the theory of trailing edge noise, J. Sound Vibr., 1978, 61(3), 437-465.
[25] Guo Y.P., Flap side edge noise modeling and prediction, J. Sound Vibr., 2013, 332(5), 3856-3868.
[26] Brooks T.F., Humphreys W.M., Flap-edge aeroacoustic measurements and predictions, J. Sound Vibr., 2003, 261(1), 31-74.
[27] Dobrzynski W., Pott-Pollenske M., Slat noise source studies for farfield noise prediction, Proc. 7th AIAA/CEAS Aeroacoustics Conference, (Maastricht, NL), May 28-30, 2001.
[28] Guo Y.P., Slat noise modeling and prediction, J. Sound Vibr., 2013, 331(15), 3567-3586.
[29] Guo Y.P., A statistical model for landing gear noise prediction, J. Sound Vibr., 2005, 282(1-2), 61-87.
[30] Gupta V.H., Munjal M.L., On numerical prediction of the acoustic source characteristics of an engine exhaust system, J. Acoust. Soc. Amer., 1992, 92(5), 2716-2725.
[31] Albertson F., Gilbert J., Harmonic balance method used for calculating the steady state oscillations of a simple once-cylinder cold engine, J. Sound Vibr., 2001, 241(4), 541-565.
[32] Davies P.O.A.L., Harrison M.F., Predictive acoustic modelling applied to the control of intake/exhaust noise noise of IC engines, J. Sound Vibr., 1997, 202(2), 249-274.
[33] Takagi S., Nakamura T., Irie Y., A modeling of nonlinear wave propagation in engine exhaust systems, Proc. Inter-Noise 84, (Honolulu, HI), 1984.
[34] Thurston D.B., Design for flying, 1978, McGraw-Hill, New York.
[35] Dobrzynski W., Vogelsang B.M., Emissionskennwerte von Propellerflugzeugen fur Schallimmissionsrechnungen an Landplatzen, Proc. DAGA 94, (Dresden, Germany), 1994, 405-408.
[36] Tada H., An intermittent-combustion general aviation aircraft engine exhaust noise prediction algorithm. Embry-Riddle Aeronautical University, Daytona Beach, FL, 1999.
[37] Moshkov P.A., Integral model of noise of an engine-propeller power-plant, J. Eng. Phys. Thermophys., 2018, 91(2), 332-338.
[38] Lim T.C., Singh R., Statistical energy analysis of a gearbox with emphasis on bearing path, Noise Control Eng. J., 1991, 37(2), 63-69.
[39] Lim T.C., Singh R., Vibration transmission through rolling element bearings - part IV: statistical energy analysis, J. Sound Vibr., 1992, 153(1), 37-50.
[40] Miller L.N., Wood E.W., Hoover R.M., Thompson A.R., Patterson S.L., Electric power plant environmental noise guide, 1984, Edison Electric Institute, Washington D.C.
[41] Bies D.A., Hansen C.H., Engineering noise control, 2003, Spon Press, London.
[42] Joint Department of the Army, Air Force and Navy, Noise and vibration control for mechanical equipment - Technical manual TM5-805-4/AFM 88- 37/NAVFAC DM-3.10, 1980.
[43] Bruce R.D., Moritz C.T., Bommer A.S., Handbook of noise and vibration control, ch. Sound power level predictions for industrial machinery, 2007, 1001-1009, Hoboken, John Wiley & Sons, Inc.
[44] Official Journal of the European Union, Regulation No. 598/2014 of the European Parliament and Council on the establishment of rules and procedures with regard to the introduction of noise-related operating restrictions at Union airports within a balanced approach, 2014, 65-78.
[45] Riboldi C.E.D., Bigoni F., Salucci F., Rolando A., Trainelli L., Switching to electric propulsion: fleet and infrastructure sizing, Proc. 25th Int. Congr. Italian Association of Aeronautics and Astronautics, (Rome, Italy), Sep 9-12, 2019.
[46] Cessna Aircraft Company, Textron Inc., One Cessna Boulevard, Wichita, KS 67215, cessna.txtav.com.
[47] ECAC, Report on standard method for computing noise contours around civil airports - Volume 3: Reference Cases and Verification Framework. Neuillysur- Seine, France, 2016.

[48] Smith M.H., A prediction procedure for propeller aircraft flyover noise based on empirical data, SAE Trans., 1981, 90(2), 2114-2124.
[49] Royal Aeronautical Society, Airframe noise prediction - ESDU 90023, 1990.
[50] SAE Aerospace, Procedure for the calculation of airplane noise in the vicinity of airports - AIR 1845, 1986.
[51] Yacovitch T.I., Yu Z., Herndon S.C., Miake- Lye R., Liscinsky D., Knighton W.B., Kenney M., Schoonard C., Pringle P., Exhaust emissions from in-use general aviation aircraft, Res. Rep. 164, ACRP, 2016.
[52] Piper Aircraft Inc., 2926 Piper Dr, Vero Beach, FL 32960, www.piper.com.
[53] Beechcraft, Textron Inc., 10511 E Central Ave Wichita, KS 67206, beechcraft.txtav.com/en.
[54] MAHEPA, Modular Approach to Hybrid-Electric Propulsion. EU H2020 Research and Innovation Program, Grant N.723368, 2017-2021.
[55] Pipistrel Vertical Solutions d.o.o., Goriska Cesta 50a, SI–5270 Ajdovščina, Slovenia, www.pipistrel.si.
[56] BRP-Rotax, Rotaxstrasse, 1 4623 Gunskirchen, Austria.
[57] Lycoming Engines, 652 Oliver Street, Williamsport, PA 17701.